Energy Correlation of the Three Electrons Emitted during the Triple Photoionization of Ar

Y. Hikosaka,[1] P. Lablanquie,[2,3] F. Penent,[2,3] T. Kaneyasu,[1] E. Shigemasa,[1] R. Feifel,[4] J. H. D. Eland,[5] and K. Ito[6]

[1]*UVSOR Facility, Institute for Molecular Science, Okazaki 444-8585, Japan*
[2]*UPMC, Université Paris 06, LCPMR, 11 rue Pierre et Marie Curie, 75231 Paris Cedex 05, France*
[3]*CNRS, LCPMR (UMR 7614), 11 rue Pierre et Marie Curie, 75231 Paris Cedex 05, France*
[4]*Department of Physics and Material Sciences, Uppsala University, S-751 21 Uppsala, Sweden*
[5]*Physical and Theoretical Chemistry Laboratory, South Parks Road, Oxford, OX1 3QZ, United Kingdom*
[6]*Photon Factory, Institute of Materials Structure Science, Oho, Tsukuba 305-0801, Japan*

(Received 4 September 2008; published 5 January 2009)

We report on an experimental investigation of energy correlation among three electrons emitted in valence triple photoionization (TPI) of Ar. The energy correlations reveal a predominant contribution from sequential TPI processes involving intermediate Ar^{2+} formation, which suggests that such indirect contributions should be included in the formulation of the threshold law for TPI cross sections. The differential cross section for direct TPI at about 150 eV above threshold producing one slow electron with a few eV kinetic energy is found to have a deeply hollow *U*-shaped profile in energy sharing between the other two electrons.

DOI: 10.1103/PhysRevLett.102.013002 PACS numbers: 32.80.Fb, 33.60.+q

Multibody Coulomb interaction in multiple photoionization of atoms and molecules has become a growing field of research in recent years. Even for double photoionization (DPI) of two-electron atomic systems, which are the simplest cases of multiple photoionization, the resultant three-body Coulomb problem cannot be solved analytically. Because of the massive experimental and theoretical efforts exerted over the past two decades, our understanding of this prototype multiple photoionization process has improved very significantly [1,2].

Comparatively little attention has been paid so far to the four-body Coulomb problem which arises in the triple photoionization (TPI) of atoms. While TPI of Li is the prototype of the four-body Coulomb problem [3], it has the peculiarity of being associated with electron emissions from two different shells. In contrast, TPI from the same valence orbitals, which can occur, for example, in a rare gas atom like Ar, lacks this complication and thus can play a benchmark role in investigations of the four-body Coulomb problem [4,5]. So far, experimental studies on TPI have been limited to the total TPI cross sections which can be studied by photoion spectroscopy. In these studies, the main focus has been on the energy ranges near TPI thresholds [4–9]. The experimental cross sections are in essential agreement with the Wannier threshold law [10,11], but also show some deviations from it, in response to which modified threshold laws have been suggested [7–9,12]. Much deeper insights into TPI dynamics can be gained from energy and angular correlations among the three outgoing electrons. While some theoretical studies on this topic have already been reported [13–17], to the best of our knowledge, no experimental study has yet succeeded in observing energy or angular correlations in TPI. This may be related to the fact that such studies require a highly sensitive multielectron coincidence experiment, because of the extremely small TPI cross sections.

In this Letter, we report the first experimental observation of energy correlations among three valence electrons emitted in TPI, which marks an important step forward in the study of multiple photoionization processes. The present observations were achieved for TPI of Ar using a state-of-the-art multielectron coincidence method [18,19]. The spectra reveal that sequential TPI processes via intermediate Ar^{2+} formation contribute dominantly to the total TPI cross sections at the measured photon energies. The direct and indirect mechanisms can be distinguished, and we have extracted the first differential cross sections for the direct TPI process.

The experiments were performed at the undulator beam line BL-16A of the Photon Factory. Single bunch operation of the storage ring provided a 624 ns repetition period for the 200-ps-wide light pulses. Synchrotron radiation was monochromatized by a grazing incidence monochromator using a varied-line-spacing plane grating, and the photon bandwidth was set at 30 meV. A mechanical chopper in the form of a cylinder with 100 slots was employed to reduce the light repetition rate, by admitting one light pulse in every 12 μs period to the interaction region of our spectrometer [20]. Multicoincidences were recorded between electrons and analyzed in energy by their flight times in a magnetic bottle electron spectrometer [18]. The description of the analyzer and the data accumulation scheme are given elsewhere [19,20]. Calibration of the conversion from electron flight time to energy was achieved by measuring conventional He 1*s* photoelectron lines at different photon energies. It was estimated that the energy resolving power of the apparatus, $E/\Delta E$, was nearly constant at ~ 60 for electrons of $E > 5$ eV, though, for electrons of $E < 5$ eV, ΔE was limited to ~ 20 meV. It was also estimated

that the detection efficiency was constant at ~60% for electrons of less than 200 eV [21].

The TPI cross section as a fraction of the total ionization cross section gradually increases from the threshold (84.124 eV [22]), before it reaches a plateau (~2%) starting around $h\nu = 200$ eV [23]. The plateau continues up to the $2p$-to-Rydberg excitation range. In order to get a favorable coincidence rate for TPI, we accumulated coincidence data sets at two photon energies, $h\nu = 199.5$ and 234.7 eV, around the plateau range. Figure 1 shows the triple coincidence yields as a function of $E_1 + E_2 + E_3$, extracted from the data set accumulated at $h\nu = 234.7$ eV. Here, E_1, E_2, and E_3 denote the kinetic energies of the first (fastest), second (medium energetic), and third (slowest) electrons to arrive at the detector. The coincidence yield curve is plotted also as a function of the Ar^{3+} binding energy with respect to the neutral ground state. Three overlapping peaks are seen in the binding energy range 82–91 eV, sitting on a background of false coincidences. These peaks can be identified as the levels arising from the $3p^{-3}$ configuration [22]. The intensity ratios of the ^4S, ^2D, and ^2P peaks in Fig. 1 are found to be 1.1:1.4:1 by a least-squares fitting using a sum of Gaussian functions; they change slightly to 1.1:1.8:1 at $h\nu = 199.5$ eV. These ratios do not agree with the statistical weights of 0.67:1.67:1 as ^4S formation is particularly enhanced in the present observations. In addition to these first three clear peaks, weak structures assigned to the $Ar^{3+}(3s^{-1}3p^{-2})$ states are discernible in the binding energy range of 97–109 eV of Fig. 1.

Figure 2 represents the energy distributions among three electrons, where the vertical axes correspond to E_3 and the horizontal ones to $E_1 - E_2$. These maps have been extracted from the data set accumulated at $h\nu = 234.7$ eV, by restricting $E_1 + E_2 + E_3$ to the four ranges indicated in Fig. 1. The $E_1 + E_2 + E_3$ ranges for Figs. 2(a)–2(c) correspond to the formation of individual Ar^{3+} states, while the one in Fig. 2(d) corresponds to the false coincidence background. The way of plotting is equivalent to the Dalitz plot [24], and compacts the energy distributions of the three electrons. All the maps show strong enhancements around $E_1 - E_2 = 150$ eV and $E_3 = 0$ eV, which are due predominantly to false coincidences including two slow (near 0 eV) electrons. Unfortunately, such false coincidences are very intense as compared to the true coincidence events from TPI with its inherently low branching ratio.

A prominent horizontal stripe is visible in Fig. 2(c) at $E_3 = 2.2$ eV. In addition, closer inspection identifies similar, but weaker, horizontal stripes in Figs. 2(a)–2(c). The curves in the right-hand panels, which are the projections of the yields on the maps onto the vertical axes, exhibit the peaks corresponding to the horizontal stripes. In contrast, no such stripe is discernible in Fig. 2(d), which implies that the horizontal structures are due to TPI of Ar. Each hori-

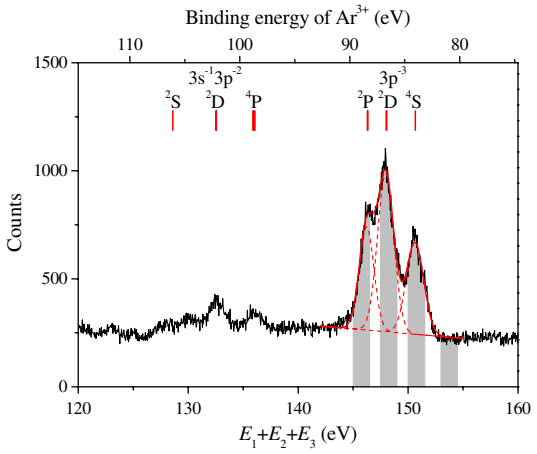

FIG. 1 (color online). Distributions of the kinetic energy sum for three electrons detected in coincidence, extracted from the coincidence data set accumulated at $h\nu = 234.7$ eV. The accumulation time was 12 h, at count rates below 3000 Hz. True triple coincidence rate is around 1.5 Hz. A scale showing binding energy with respect to the neutral ground state is included at the top, and Ar^{3+} levels are indicated with bars [22]. The four energy ranges used for extraction of the energy correlation maps in Fig. 2 are indicated by shading.

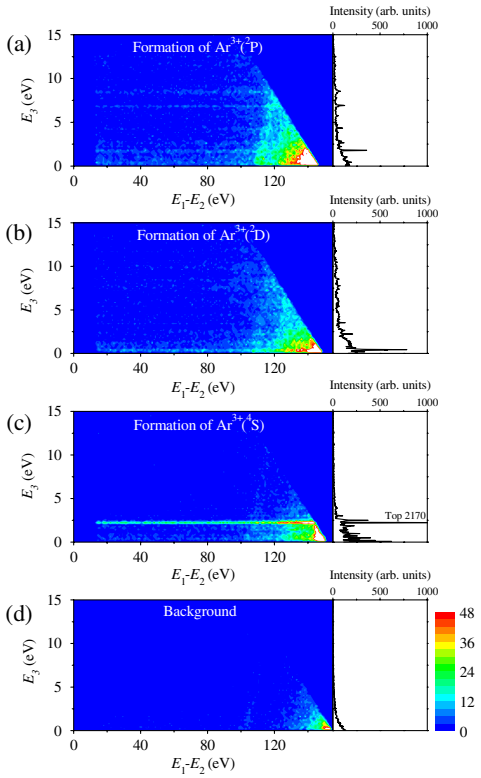

FIG. 2 (color online). Two-dimensional maps of correlations among three electrons, where the sums of the three electrons are restricted to the ranges for the formation of (a) $Ar^{3+}(3p^{-3}{}^2P)$, (b) $Ar^{3+}(3p^{-3}{}^2D)$, and (c) $Ar^{3+}(3p^{-3}{}^4S)$ and (d) to a background range. The ranges for these choices are indicated in Fig. 1. Intensities are plotted on a common linear scale. The areas of $E_1 - E_2 < 14$ eV are blind due to the detection dead time arising from inseparable electron signals. The right-hand panels show projections of the yields on the maps onto the vertical axes.

zontal stripe can be attributed to a sequential TPI process in which the slowest electron is emitted with a fixed energy and the other electrons have distributed energies. Direct TPI can hardly be seen on the maps, as the expected smooth distributions can produce only low-contrast features.

Figure 3 shows the E_3 distributions for formation of the $Ar^{3+}(3p^{-3})$ states at $h\nu = 234.7$ [solid (black) lines] and 199.5 eV [dashed (red) lines]. The E_3 distributions at the two photon energies for each final Ar^{3+} state formation agree precisely in the positions of the sharp peaks. This agreement demonstrates that the horizontal stripes in Fig. 2 are associated with initial DPI followed by autoionization of the Ar^{2+} states formed. If the peaks were due to single photoionization into Ar^{+} states, they should move as a function of photon energy. The sharp peaks in Fig. 3 can thus be assigned to autoionization of Ar^{2+} into Ar^{3+}; in fact, the energies of some peaks agree with Ar^{2+} autoionization energies observed in the Auger decay of $Ar^{+}(2p^{-1})$ [25]. For example, the most intense peak at $E_3 = 2.2$ eV in Fig. 3(c) can be assigned to the autoionization of a $3s^{-2}$ satellite state with a $3p^{-4}3d^2$ configuration [25,26]. The energy distribution of the two photoelectrons emitted in formation of this Ar^{2+} state is shown in Fig. 4(a). This distribution reflects the coincidence yields along the horizontal stripe seen at $E_3 = 2.2$ eV in Fig. 2(c). It shows a continuous profile increasing gradually toward the minimum and maximum energies. Such a U-shaped profile is expected in direct DPI [27], and it agrees well with those we observed in Ne valence DPI with similar available energies [21]; the profile thus confirms that the Ar^{2+} state is produced essentially by direct DPI. No sharp peaks denoting sequential DPI are visible in the distribution, but weak peaks might be hidden by the limited statistics.

In Fig. 3(c), the majority of sharp peaks lie below 2.4 eV, which is the energy difference between $Ar^{3+}(3p^{-3}{}^2D)$ and $Ar^{3+}(3p^{-3}{}^4S)$. This observation indicates that most of the peaks in this region, except for the large peak at $E_3 = 2.2$ eV, correspond to Rydberg states converging to $Ar^{3+}(3p^{-3}{}^2D)$. Similar features at higher energies, probably due to the Rydberg states converging to $Ar^{3+}(3p^{-3}{}^2P)$,

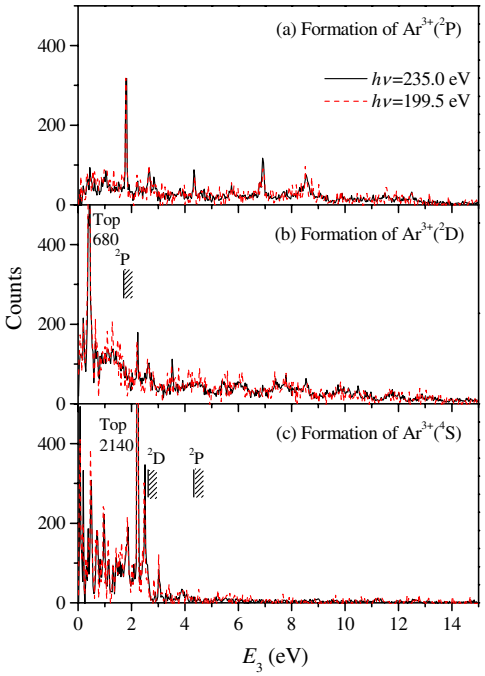

FIG. 3 (color online). Net distributions of slowest electrons for the formation of (a) $Ar^{3+}(3p^{-3}{}^2P)$, (b) $Ar^{3+}(3p^{-3}{}^2D)$, and (c) $Ar^{3+}(3p^{-3}{}^4S)$, where the false contributions have been subtracted. The false contributions are assumed to be the same as the distribution in the right panel of Fig. 2(d) and to have the background intensities seen in Fig. 1. The curves that are solid (black) and dashed (red) are deduced from the data sets accumulated at $h\nu = 234.7$ and 199.5 eV, respectively. The counts in the dashed (red) curves are magnified by a factor of 4.5, for comparison. Discretization by 30 meV step was adopted for all the distributions.

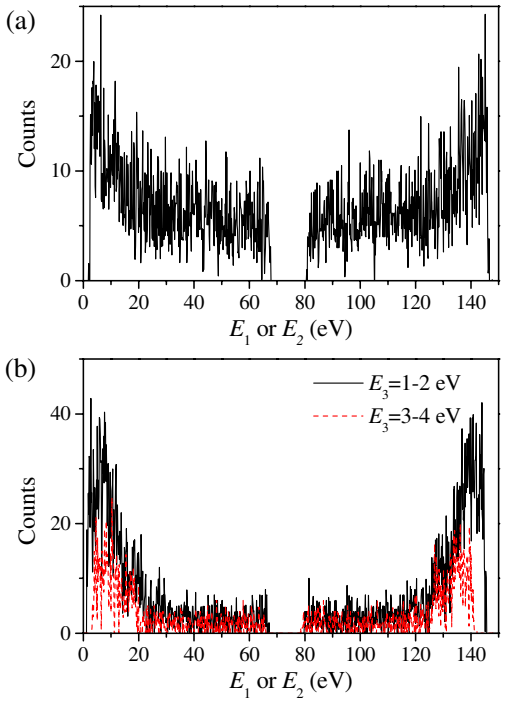

FIG. 4 (color online). (a) Kinetic energy distribution of the two photoelectrons emitted in DPI into an $Ar^{2+}(3s^{-2})$ satellite state, which reflects the coincidence yields for the horizontal stripe at $E_3 = 2.2$ eV in Fig. 2(c). The false contribution estimated from the distribution at a vicinal E_3 range (2.03–2.14 eV) was subtracted. (b) Kinetic energy distributions of the two electrons emitted with electrons in $E_3 = 1$–2 eV [solid (black) lines] and 3–4 eV [dashed (red) lines] in TPI into $Ar^{2+}(3p^{-3}{}^2D)$. The contributions from false coincidences were subtracted by assuming that the false contribution profiles are described by the distributions extracted for the same E_3 ranges and the background $E_1 + E_2 + E_3$ range indicated in Fig. 1. The gaps seen in the middle and both extremes of all the curves are due to the detection dead time arising from inseparable electron signals. Discretization by 150 meV step was adopted for all the distributions.

are seen in Figs. 3(b) and 3(c), but they are less pronounced as compared to the Rydberg structure related to $Ar^{3+}(3p^{-3}{}^2D)$. The fact that the formation of Rydberg states converging to $Ar^{3+}(3p^{-3}{}^2D)$ is more favorable than formation of states converging to $Ar^{3+}(3p^{-3}{}^2P)$ suggests that direct TPI into $Ar^{3+}(3p^{-3}{}^2D)$ is also more intense than that into $Ar^{3+}(3p^{-3}{}^2P)$. This is because DPI into a Rydberg-type Ar^{2+} state can be regarded as an extreme case of the direct TPI process, where one of the three photoelectrons has too little energy to escape and is trapped in a Rydberg orbital.

It is expected that direct TPI should result in smooth structures underlying the sharp peaks in Fig. 3, because the available energy for the formation of the individual Ar^{3+} state is shared continuously by the three photoelectrons. Indirect TPI processes forming sharp peaks may also contribute weakly to the smooth structures in the E_3 range below the peak energies, because the autoionization electrons could be detected as the middle energy ones. The relative intensities of the smooth underlying continua in Fig. 3 indicate that direct TPI is strongest in the ^2D channel, less strong in the ^2P channel and weak in the ^4S channel. The more intense direct TPI in the ^2D channel than in the other channels is thus in accord with the intensity of the corresponding Rydberg features.

Figure 4(b) plots the energy distributions of the two faster electrons emitted in formation $Ar^{3+}(3p^{-3}{}^2D)$, for events selected by restricting the slowest electron energy to $E_3 = 1$–2 eV and 3–4 eV. Although weak peak structures are discernible in these restricted E_3 ranges in Fig. 3(b), we believe that most of the selected intensity can be attributed to direct TPI. The distributions again show U-shaped profiles, but the profiles are more enhanced around the maximum and minimum energies, as compared with the U-shaped profile in Fig. 4(a). The observed distributions show that for the emission of a low energy electron, a highly unequal energy sharing is favored for the other two electrons. One possible interpretation of this unequal energy sharing is that emission of a high energy photoelectron is accompanied by an emission of two slow electrons in a process of ''double shakeoff''. Theoretical calculations have predicted such U-shaped distributions in TPI of Li with the available energies of 116.5 eV [14] and 115 eV [16]; the present observation qualitatively confirms these theoretical predictions.

In conclusion, we have observed for the first time the energy distributions among three electrons emitted in TPI of Ar, with a state-of-the-art multielectron coincidence method. We have observed a predominant contribution from indirect TPI via intermediate Ar^{2+} formation. Although the experiments were performed, for practical coincidence rate reasons, at photon energies far from the TPI threshold, the same indirect TPI can be expected to contribute significantly to the cross section in near-threshold ionization. Such contributions may be the source of the observed deviation [5] from the Wannier threshold law, as has been predicted by Gribakin, Sahoo, and Ostrovsky [9]. Furthermore, double differential cross sections for direct TPI at 150 eV excess energy are found to present a deeply hollow U-shaped profile, when the energy of one of the electrons is fixed at low energy. This is the first experimental visualization of the direct triple escape dynamics. Comparison with theoretical calculations should bring more detailed understanding of direct TPI dynamics; no directly relevant calculation is available for the present case and we strongly hope that our data may stimulate such a theoretical effort.

The authors thank P. Selles for fruitful discussions. We are grateful to the Photon Factory staff for the stable operation of the PF ring. Financial support from JSPS and CNRS is acknowledged. J. H. D. E. thanks the Leverhulme Trust for support. R. F. thanks VR for support. This work was performed with the approval of the Photon Factory Advisory Committee (Proposal No. 2006G230).

[1] J. S. Briggs and V. Schmidt, J. Phys. B **33**, R1 (2000).
[2] L. Avaldi and A. Huetz, J. Phys. B **38**, S861 (2005).
[3] P. N. Juranic and R. Wehlitz, Phys. Rev. A **78**, 033401 (2008).
[4] J. A. R. Samson and G. C. Angel, Phys. Rev. Lett. **61**, 1584 (1988).
[5] J. B. Bluett, D. Lukić, and R. Wehlitz, Phys. Rev. A **69**, 042717 (2004).
[6] R. Wehlitz *et al.*, Phys. Rev. A **61**, 030704(R) (2000).
[7] J. M. Feagin and R. D. Filipczyk, Phys. Rev. Lett. **64**, 384 (1990).
[8] T. Pattard and J. M. Rost, Phys. Rev. Lett. **80**, 5081 (1998).
[9] G. F. Gribakin, S. Sahoo, and V. N. Ostrovsky, Phys. Rev. A **70**, 062717 (2004).
[10] G. H. Wannier, Phys. Rev. **90**, 817 (1953).
[11] G. H. Wannier, Phys. Rev. **100**, 1180 (1955).
[12] A. Emmanouilidou and J. M Rost, J. Phys. B **39**, 4037 (2006).
[13] A. W. Malcherek, J. M. Rost, and J. S. Briggs, Phys. Rev. A **55**, R3979 (1997).
[14] J. Colgan and M. S. Pindzola, J. Phys. B **39**, 1879 (2006).
[15] A. Emmanouilidou and J. M. Rost, J. Phys. B **39**, L99 (2006).
[16] A. Emmanouilidou, Phys. Rev. A **75**, 042702 (2007).
[17] A. Emmanouilidou, P. Wang, and J. M Rost, Phys. Rev. Lett. **100**, 063002 (2008).
[18] J. H. D. Eland *et al.*, Phys. Rev. Lett. **90**, 053003 (2003).
[19] Y. Hikosaka *et al.*, Phys. Rev. Lett. **97**, 053003 (2006).
[20] K. Ito *et al.* (to be published).
[21] T. Kaneyasu *et al.*, Phys. Rev. A **76**, 012717 (2007).
[22] National Institute of Standards and Technology, NIST Atomic Spectra Database Energy Levels, Available: http://physics.nist.gov/PhysRefData/ASD/levels_form.html.
[23] N. Saito and I. H. Suzuki, Int. J. Mass Spectrom. Ion Processes **115**, 157 (1992).
[24] R. H. Dalitz, Philos. Mag. **44**, 1068 (1953).
[25] P. Lablanquie *et al.*, J. Electron Spectrosc. Relat. Phenom. **156–158**, 51 (2007).
[26] H. Pulkkinen *et al.*, J. Phys. B **29**, 3033 (1996).
[27] R. Wehlitz, Phys. Rev. Lett. **67**, 3764 (1991).